On the Estimation of Three-Dimensional Porosity of Insect-Proof Screens

F.-J. Granados-Ortiz[a], F.M. Arrabal-Campos[b,c], A. Lopez-Martinez[b,c,*], F.D. Molina-Aiz[b,c], A. Peña-Fernández[b,c], D.L. Valera[b,c]

[a]Department of Mechanical, Thermal and Fluid Engineering, University of Málaga
C/ Dr Ortiz Ramos s/n, 29071 Málaga, Spain

[b]Department of Engineering, University of Almería, Almería, Spain

[c]CIAIMBITAL Research Centre, University of Almería, Almería, Spain

[*]Corresponding author: alexlopez@ual.es

Abstract

The two-dimensional estimation is the approach to porosity par excellence in the literature of insect-proof screens for their geometric characterisation and estimation of their aerodynamic parameters. However, this is not an accurate estimation, since the geometry of insect-proof screens consists of interlaced threads that create a three-dimensional woven structure, leading to different thicknesses and overlapping of threads. This paper suggests a mathematical approach to reconstruct computationally the 3D structure of the screens and to estimate the volumetric porosity, relying solely on easily measurable quantities such as diameter of threads, spacing of threads and thickness. The results on the application to 20+6 insect-proof screens in this work evidence that the suggested approach outperforms the standard two-dimensional modelling. These results also support experimental observations in the relationship between porosity and pressure drop not explainable by the two-dimensional approach. To increase the reliability on the analysis of porosity, the propagation of experimental uncertainty has been also included in the comparison between brand new and old&washed insect-proof screens. A software (Poro3D v1.0) using the methodology developed in this work is provided as supplementary material to this manuscript to instantly obtain both 3D and 2D porosities, as well as the reconstruction of 3D geometries.

Keywords: Insect-proof screens, Porosity, Aerodynamic characterisation, Woven fabric, Parametric surfaces

1. Introduction

Insect-proof screens are a physical method of crop protection that in recent decades has been extended and implemented in many countries, especially in Spain [1]. The textile industry estab-

lished the designation warp and weft because the screens are manufactured on totally flat looms. The width of the mesh is determined by the threads that are fixed on the loom, hence the name warp. The warp threads are divided into two groups of threads. The alternate separation set for these threads allows the shuttle to slide through the mesh crossing other threads called weft. In this way the loom is woven. They are installed in the lateral and zenithal ventilation openings of greenhouses, in order to prevent or reduce the entry of insects into the interior. Therefore, the choice of the type of insect-proof screen is conditioned by the size of the smaller pest species, whose presence inside the greenhouse is to be avoided [2].

Reducing insect populations inside a greenhouse provides great benefits by limiting direct damage to crops and disease transmissions, where insects are the main vectors of these diseases [3]. Another benefit derived is the reduction of treatment with phytosanitaries [4, 5], since this reduction of insect population is proportional to the quantity supplied for crop control [6, 7].

The use of insect-proof screens inside a greenhouse generates some problems related to ventilation, because it can be considered as an aerodynamic resistance. This yields that the exchange with the exterior is reduced and the bioclimatic environment [8, 9, 10, 11] inside the greenhouse is misaligned. This problem leads to a late development of the crop [12] and produces a favorable environment for the growth of fungal diseases [13, 14].

The physical description of the ventilation flow inside a greenhouse depends on the window geometry and the woven geometry of the insect-proof screen, as studied in [11, 15, 16, 17, 18] . This produces a pressure drop due to the circulation of air flow through a porous media. The pressure drop produced by insect-proof screens can be described by a quadratic relationship [15] dependent on the flow velocity (u). From this approximation, the aerodynamic behavior of the screen used can be determined by obtaining three experimental parameters F_ϕ, K_p and Y, where F_ϕ is pressure drop coefficient, K_p is the permeability and Y is the inertial factor.

The aerodynamic characteristics are estimated by performing wind tunnel tests. With these experiments, it is possible to develop models for predicting the pressure drop coefficient (F_ϕ) from the Reynolds number (Re_d) as a function of the average diameter of threads (D_h) and porosity (ϕ) [19]. These geometric parameters D_h and ϕ_{2D} (two-dimensional porosity) can be determined by digital image processing of insect-proof screens using computer vision techniques [20]. Actually, both geometrical parameters have been successfully measured in [21]. However, the direct measurement method is only valid to obtain the thread diameter and thickness of

the screen. A micrometer can be used to do this measurement. With the characteristics from production process parameters and the diameter obtained, the porosity can be estimated [22].

Recent studies have developed different models to estimate the pressure drop caused by an insect-proof screen at a specific air velocity from its geometric characteristics. The pressure drop coefficient is estimated as a function of porosity and two options for the Reynolds number. The Reynolds number is a critical parameter, since it can be calculated whether from the wire diameter or from of the thickness [23]. The permeability and inertia factor can also be estimated from different geometric parameters (K_p as a function of thread diameter and porosity; Y as a function of thread diameter, and the inner pore diameter), and then K_p and Y can be used to obtain the value of pressure drop [23]. These models have improved the estimation of these parameters compared to previous models described in the literature [23]. However, this improvement is limited by the estimation of the different geometric parameters required. Moreover, in the literature, screen aerodynamics are entirely based on 2D porosity. However, a 3D porosity modeling of the screen may overcome this limiting estimation by improving the characterisation.

There is an important dearth of literature on the 3D consideration of insect-proof screens. Most works in the literature have considered screens as planar surfaces, as a consequence of orthogonal projection [21, 23, 24], which is a simplification due to the complexity of their 3D structure. Actually, three-dimensional efforts to date have been conducted to the calculation of the area of the porous, leaving an accurate estimation of porosity behind, due to the interest in quantifying the resistance to the pass of air through the porous openings. For instance, in [25] was proposed to calculate the area of the porous from the orthogonally projected area of the 3D structure inside the porous. This approximation yielded high errors due to the non-linearity of the hyperbolic paraboloid real area. An improvement of this calculation was carried out in [26] for insect-proof screens. In this work, it was proposed an alternative method for estimating the area of a three-dimensional porous. The spatial surface of the hole is defined by segments (generatrices of threads adjacent to the porous), which define a parallelepiped based on the characteristic geometric parameters L_{px} and L_{py} (horizontal spacing between threads in the x and y direction), D_{hx} and D_{hy} (diameter of threads in the x and y direction), and thickness e (see Figure 1). This method calculates the real surface improving the underestimated area of the porous in the two-dimensional approach. Regarding the correct modelling of the 3D structure, several investigations in the literature of woven fabrics proposed the use of an interlaced thread model as the work

on cloth structures developed by Peirce in [27]. This is the first work on theoretical modelling of interlaced yarns, which considers threads as incompressible with circular cross-section. Other researchers continued this work and extended the model to more advanced and complex shapes such as [28], where mechanical deformation of threads was included; or the recent work in [29], where Fourier series have been used to model the sinusoidal-like shape of very complex multi-layer threads. Structural properties of 3D woven fabrics have been also studied numerically using the Finite Element Method (FEM), see for instance [30]. A comprehensive review on the analysis of the mechanical properties of these structures can be found in [31]. Also, in other works such as [32], Computational Fluid Dynamics (CFD) are used to study the pressure drop in textile fabrics using 3D models with circular and elliptic cross-sections, which evidence the importance of the availability of 3D shapes of insect-proof screens for further computational investigation. None of the aforementioned 3D studies (except [26]) were oriented to application in insect-proof screens, and there are no works in the literature on the estimation of porosity from a 3D view. The 2D porosity modelling of screens is the standard approach even in recent applications in the literature such as e.g. [23, 24, 33, 34].

Herein, we introduce a novel solution to estimate porosity of insect-proof screens as a three-dimensional property for the first time in the literature. This estimation is grounded on the mathematical reconstruction of the porous volume and based on the measurable characteristic geometric parameters L_{px}, L_{py}, D_{hx}, D_{hy}, and e. In order to improve the reliability of this research, an analysis of the propagation of experimental uncertainty in the model has been included. The results yield that the theoretical estimations are consistent with the experimental observations. This theoretical approach will be crucial for the estimation of the aerodynamic characteristics inside a greenhouse by making accurate estimations of the physical parameters, F_ϕ, K_p and Y. In fact, this three-dimensional model sheds light on the behaviour of pressure drop observed in experimental tests (pressure drop decreases as porosity increases), not explainable by two-dimensional porosity. Thus, this approach will improve the prediction and quantification of the effectiveness of screens against insects and fungal diseases by enhancing the control of the bioclimatic environment of the crop within greenhouses. In addition, with accurate estimates of 3D porosity, and also its 3D geometric reconstruction, it will be possible to select the right type of screen to exclude a particular type of pest but aiming at a decent high porosity at the same time. The methodology and codes resulting from this work have been implemented in the Poro3D v1.0 software, which is provided

as supplementary material to this manuscript.

The present paper has been structured as follows: Section 2 is dedicated to describe the methodology pursued in this investigation. In Section 3, details on the mathematical foundations of the theoretical approach are given, covering aspects such as the model of the interlaced threads, parametrisation of the volumes, and calculation of superficial and volumetric porosity. In Section 4, the results from the application of the model to real insect-proof screens are presented. This includes the effect of ageing in the screens, by including an uncertainty quantification study. Finally, in Section 5 the most relevant conclusions from the present work are given.

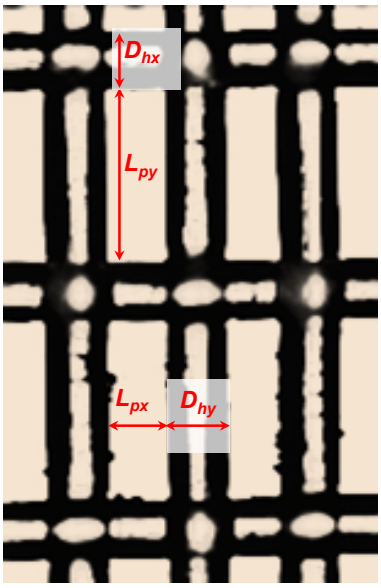

Figure 1: Dimensions of an insect-proof screen.

2. Methodology

The methodology followed in this work consists of three stages. First, the geometric parameters of the insect-proof screen under consideration are measured in the laboratory by means of microscope images (which can be processed by a dedicated software [21]). These values are input parameters to the equations to be solved numerically. Although the more the measured parameters the better, some may be hard to measure, such as the crisp of a thread or certain angles. Thus, to facilitate the measurement task, the models are adapted to require only the diameter of threads, spacing between threads, thickness of the screen, and to specify whether the outer threads are those in the x or y direction.

Second, a non-linear model is solved with an iterative approach by means of a numerical code. The code uses the geometric parameters as input and estimates the slope of the threads, the portion in contact between threads, and their total lengths. This also allows to reconstruct the three-dimensional shape of the interlacing threads, which is also provided by the numerical code for visualisation.

Third, by using the solution from the previous step, the volumetric porosity can be estimated as the ratio between the volume of threads and total volume. These volumes are calculated by means of the integral of parametrisation volumes. Since during the measurement stage experimental uncertainty has been also identified, its propagation in the model and estimation of volumetric porosity can be also quantified by means of a random/pseudo-random sampling (or any suitable sampling or quadrature-based method). This leads not only to the estimation of a value of porosity, but also the impact of experimental uncertainty in the calculation, which may be of interest in a comparison between new and old screens.

3. Mathematical Considerations

In this section, the mathematical details of the non-linear model of the threads interlacing, the parametrisation of volumes and calculation of volumetric porosity are given. The validation of the models is also included in this section.

3.1. Thread Interlacing Model

The model for cloth woven structures first suggested by Peirce [27] is used in this work. This model consists of assuming that a woven fabric is composed of inextensible, incompressible and fully round cross-section threads. This is an accurate representation for insect-proof screens, since these are regularly made of High-Density Polyethylene (HDPE) monofilament-woven fabrics [33]. Thus, the objective in this work is to adapt such mathematical model to the geometry of insect-proof screens, which are usually characterised in the literature experimentally by the diameter of the interlaced threads, their spacing and the thickness [23, 21, 33]. Peirce [27] suggested that a woven fabric can be modelled by means of seven equations connecting eleven quantities. These equations are:

$$c_i = \frac{l_i}{p_i} - 1, \tag{1}$$

$$p_i = (l_i - D\theta_i)\cos\theta_i + D\sin\theta_i \tag{2}$$

$$h_i = (l_i - D\theta_i)\sin\theta_i + D(1 - \cos\theta_i), \tag{3}$$

$$D = h_x + h_y, \tag{4}$$

where c_i is the fractional crimp, l_i is the total length of the thread, p_i is the horizontal spacing of threads, θ_i is the angle with respect to the horizontal plane, and h_i is the vertical displacement of the threads. The subscript $i = x,y$ represents a specific thread direction thread (in the present work, x is used for quantities related to the x-coordinate, and y for quantities in the y-coordinate) as shown in Figure 2).

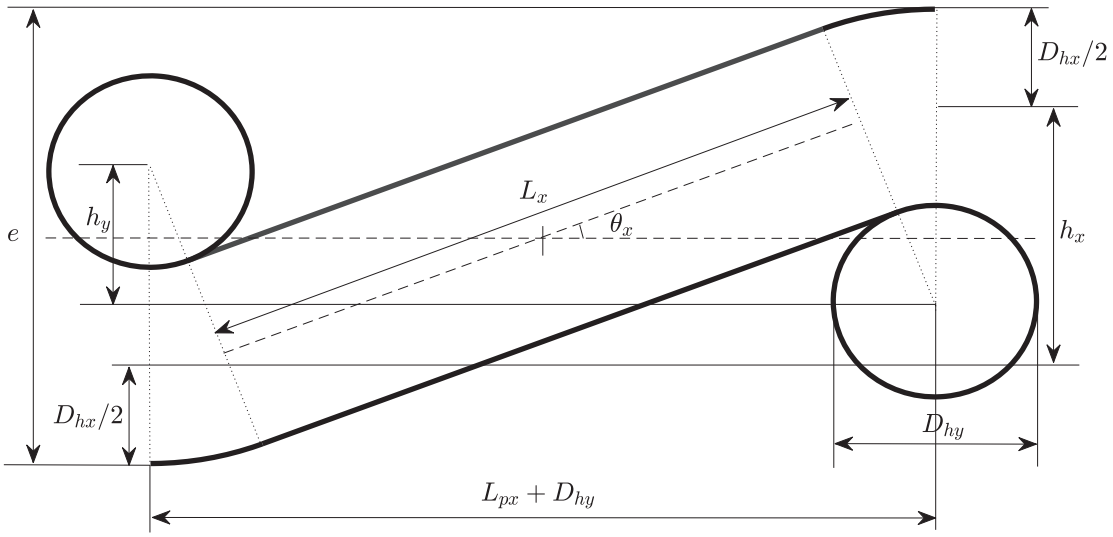

Figure 2: Sketch of Peirce's woven fabric model applied to insect-proof screens characterisation.

Amongst the eleven quantities required to fully describe the geometry of the threads, only the spacings p_i (in Figure 2 can be seen that $p_y = L_{px} + D_{hy}$) are known. In previous works in the literature, authors that characterised insect-proof screens usually only rely on the diameter of the threads (D_{hx}, D_{hy}), their horizontal spacing between threads (L_{px}, L_{py}) and the thickness (e). This is so because there are actually software that provide these data from images (see for instance [21]). The total length l_i of a thread is formed by the combination of a straight part of length L_i and two curved sides enveloping the orthogonal threads. This is the reason of the equation for the crimp (Equation (1)). To closure the mathematical problem, for instance in Equation (1) the crimp or total length should be known, but these quantities are complex to be obtained experimentally. Also, the process may be cumbersome if many insect-proof screens are under study without a dedicated software to measure l_i.

An efficient alternative is to estimate the values of the vertical distances h_x and h_y based solely on the thickness of the screen and the configuration. Alternative forms of the two equations compacted in Equation (3) can be found by trigonometric relations in Figure 2, yielding:

$$h_y = \frac{(D_{hx} + D_{hy})}{\cos\theta_x} - (L_{px} + D_{hy})\tan\theta_x, \tag{5}$$

$$h_x = (D_{hx} + D_{hy})(1 - \frac{1}{\cos\theta_x}) + (L_{px} + D_{hy})\tan\theta_x. \tag{6}$$

By using these equations, one can get rid of Equation (4). However, h_x and h_y are still unknown. Although these parameters can be related to the thickness e in Figure 2, this cannot be generalised for any insect-proof screen. This is because if the top and bottom threads (outer threads) are those that correspond to the orthogonal threads denoted by $i = y$, then the relations are different. This is depicted in Figure 3. For this reason, to closure the problem by obtaining h_x and h_y with relations with the thickness e, the practitioner must classify beforehand whether the insect-proof screen corresponds to *configuration 1* (Figure 2) or *configuration 2* (Figure 3). As rule of thumb, the *configuration 1* is also valid if both threads are at the same height. If the type of configuration is not provided, the system of equations would not have a unique solution for $\theta_i \in [0, 2\pi)$. The relations to calculate h_x and h_y are thus:

Configuration 1:

$$\begin{aligned} h_x &= e - D_{hx}, \\ h_y &= 2D_{hx} + D_{hy} - e, \end{aligned} \tag{7}$$

Configuration 2:

$$\begin{aligned} h_x &= 2D_{hy} + D_{hx} - e, \\ h_y &= e - D_{hy}. \end{aligned} \tag{8}$$

Obviously, another simple and equivalent solution could be to only consider, for instance the expressions given for *configuration 1*, and select the thread indices i accordingly. However, in many insect-proof screens, the pores are rectangles longer in the y-axis than the x-axis, thus the subscript of the threads is assumed to be known beforehand.

With all the aforementioned reductions on the model equations, it is now possible to solve the system of non-linear equations. For this task, a MATLAB script is coded, which solves the system of non-linear equations iteratively with a convergence criteria of 10^{-10}. The code has been

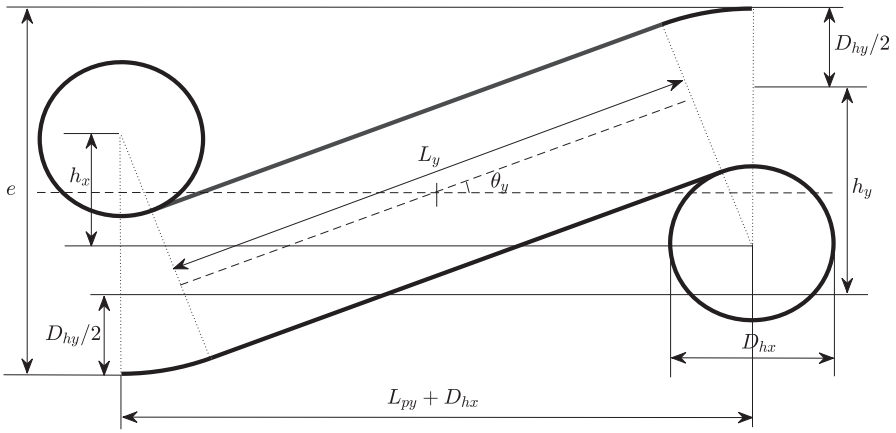

Figure 3: Example of y-axis threads ($i = y$) on top and bottom (outer threads) of the insect-proof screen (namely configuration 2).

validated with images from the laboratory, as will be also shown in Section 3.2 after introducing all the aspects of the code.

Once the script provides the geometric values, the volumes can be parametrised. Specially important are θ_x and θ_y for this objective, since these values set the slope of the straight portion of the thread and the portion of curved envelopes on the warp threads, as will be shown next.

3.2. Parametrisation of Threads.

In order to calculate the volumetric porosity, the geometry of the threads has been parametrised. This allows to visualise the correctness of the shapes, as well as to calculate the volumes of interest. These parametrisations are developed upon the solved non-linear equations with the in-house MATLAB code. The full periodic geometry consists of a cylinder with a slope θ_i, and two portions of toroids, tangential to the cross threads.

It is well-known that a cylinder of length L_i centered in the origin and around the x-axis can be expressed by using parametric equations in cylindrical coordinates as

$$\begin{aligned} x(L, s) &= L, \\ y(L, s) &= r \cos s, \text{ with } L \in [-L_i/2, L_i/2] \text{ and } s \in [0, 2\pi), \\ z(L, s) &= r \sin s, \end{aligned} \tag{9}$$

where r is the radius of the cylinder and L_i is the total length. However, the pieces of cylinder used to model the straight parts of the threads are not horizontal but have a slope θ_i (let us use θ hereinafter for the sake of simplicity). When a geometry is rotated, a rotation matrix must be

used to guarantee the conservation of the shape. For a degree of rotation θ around the y-axis, the rotation matrix obtained by considering the necessary trigonometric relations is

$$M_r = \begin{pmatrix} \cos\theta & 0 & \sin\theta \\ 0 & 1 & 0 \\ -\sin\theta & 0 & \cos\theta \end{pmatrix}. \tag{10}$$

This matrix allows to rewrite the parametric equations of the cylinder as:

$$\begin{aligned} x'(L, s) &= L\cos\theta + r\sin s\sin\theta, \\ y'(L, s) &= r\cos s, \text{ with } L \in [-L_i/2, L_i/2] \text{ and } s \in [0,\ 2\pi), \\ z'(L, s) &= r\sin s\cos\theta - L\sin\theta. \end{aligned} \tag{11}$$

In these equations the signs of the second summation terms at the right hand side of x' and y' can be inverted to consider $\theta > 0$ in the anticlockwise direction. It is obvious that the parametric equations must be customised accordingly to plot the different positions (spacing between threads) and orientations (θ_x and θ_y) of the threads.

In the geometric simplification shown in Figure 2 each thread also contains two toroid portions: one below the first orthogonal thread of diameter D_{hx}, and another above the second orthogonal thread of the same diameter. These portions of toroidal volume are concentric and tangential to the said threads, thus the reconstruction of the volume is simple once all the geometric parameters are known. For instance, in the geometry given in Figure 2, the positions of the centers of the toroids will be given by $O_1(-L_{px}/2 - D_{hy}/2,\ h_y/2)$ and $O_2(L_{px}/2 + D_{hy}/2,\ -h_y/2)$ for the first and second thread, respectively. Upon this, for instance, on a xz-plane view, the parametric equations of the portion of toroid in cylindrical coordinates can be written as

$$\begin{aligned} x'(u, v) &= (a + R\cos v)\cos u + O_{ix}, \\ y'(u, v) &= R\sin v, \text{ with } v \in [0, 2\pi) \text{ and } u \in [k,\ \theta + k), \\ z'(u, v) &= (a + R\cos v)\sin u + O_{iz}, \end{aligned} \tag{12}$$

with a the position with respect to the reference origin, R the radius of a circular section of the toroid, θ the slope of the cylinder, and O_{ix} and O_{iz} the x and z coordinates of the center of the toroid for the thread i, respectively. Must be noted that k is a parameter required to control the beginning and the end of the angle spanned by the toroid. For instance, in a sketch such as Figure 2, the first portion of toroid is developed according to $k = 3\pi/2$, and the second portion, according

to $k = \pi/2$. As in the explanation provided for the cylinder, the parametric equations of the portions of toroid must be adapted to, for instance, each y position by adding to y' the distance between threads. The process is homologous in the a yz-plane view.

By taking into account all the aforementioned parametric equations, a 3D view of the insect-proof screen thread interlacing can be reconstructed. This has been added to the numerical code, and the results are shown in Figure 4. In addition, 2D views are generated, which can be seen in Figure 5. Note that the cross section of the threads is a perfect circle, but the figure may show a elliptic-like shape due to the automatic selection of the axis limits in the visualisation of the figure. To be able to construct by parametrisation the 3D geometry is of strong interest for instance for computational design of new threads by means of Computational (Fluid) Mechanics [35, 36].

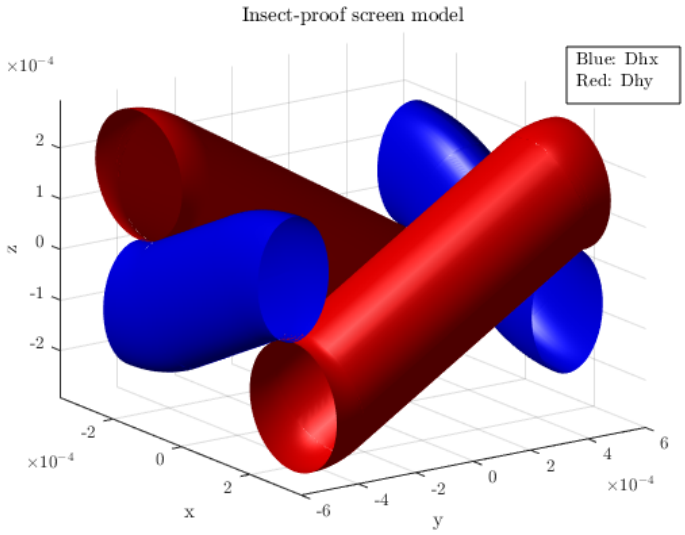

Figure 4: 3D view of the insect-proof screen threads.

A validation of the code has been developed. For a realistic validation of the thread interlacing generated, the geometric details of three insect-proof screens in Lopez et al. [23] have been input to the MATLAB code to check the accuracy in the reconstruction of real insect-proof screens. Upon experimental measurements and images taken in the laboratory, it is known that the configuration of the threads is *Configuration 2*. Several Image Recognition algorithms have been used in MATLAB to detect the edges in the microscope images (4X lens with a calibration of 10.52632 micron/pixel) of the interlaced yarns in order to perform a fair comparison. The Prewitt method calculates the gradients of the image by means of the Prewitt algorithm [37] to approximate the derivative. The regions of highest gradients are recognised as edges. Such derivatives can be

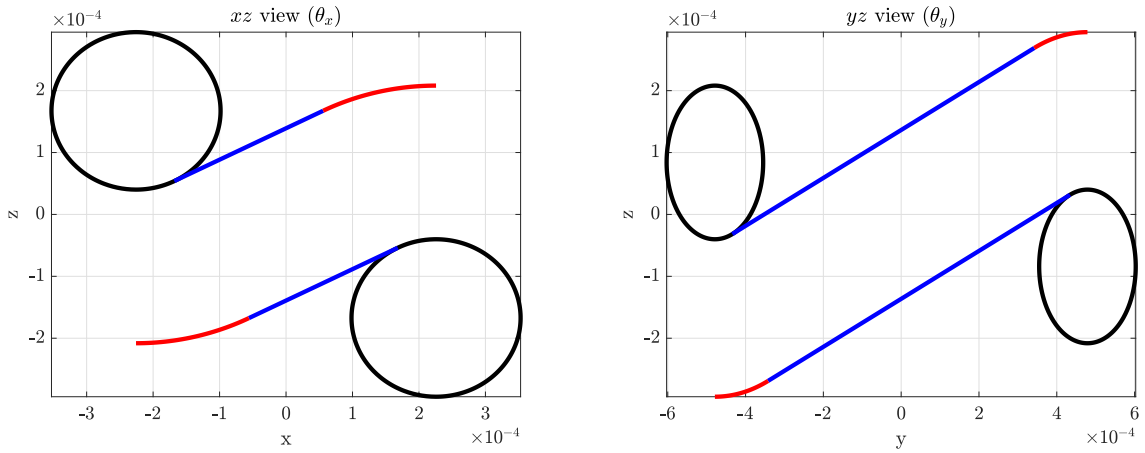

(a) xz view (b) yz view

Figure 5: 2D views of the interlacing of the insect-proof screen threads.

also approximated by the Sobel operator [38], which calculates gradient point by point with some smoothing effect of random noise; or the Roberts operator, which applies a discrete differentiation algorithm to compute the differences between adjadcent pixels [39]. The *Log* edge detection filters the image with a Laplacian of Gaussian filter (LoG), hence the name. The Gaussian filter is useful to smooth the random noise in the image, which is also another advantage in the Canny algorithm [40]. The results of the application of these algorithms are shown in Figure 6. In this figure can be seen that only the *Canny* method was able to detect the edges of the threads perpendicular to the view plane. This is because this method uses a multi-step approach with the derivatives of a Gaussian filter and detects strong and weak edges. It is the most recommended method for edge detection amongst practitioners, despite is more computationally expensive. This is the only method amongst the tested ones that is able to detect weak edges if these are connected to strong edges. This is the reason of detecting a clearer delimitation of the blurred circular sections. The mathematical details of each method are not to be described in the present manuscript, as they are used as mere tools in this work and there is a vast amount of literature on their description.

The reconstructed geometry is compared with the regular image and *Canny* edge detection method in Figure 7. In this figure, the yz view is shown (one view is enough for validation as both views depend on each other) for the regular image and edge detection. On top of these, the calculated geometry by the MATLAB code is shown in yellow and red, in order to distinguish each line. The resulting geometry shows an outstanding match with the actual insect-proof screens, despite of the assumptions of the model (round cross-section, incompressible threads, straight

threads). Must be recalled that the modelled threads are assumed to have perfect round sections, but the actual threads may have some deformation due to the tension force. Nevertheless, such change in section is not expected to be very remarkable in a HDPE yarn, as evidenced in the validation.

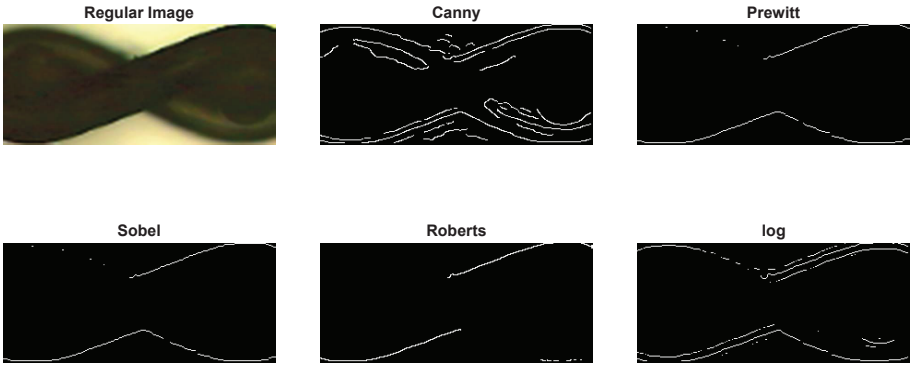

Figure 6: Detection of the edges in the image of the insect-proof screen n.1 in Lopez et al. [23]

3.3. Calculation of Volumetric Porosity

Previous works in the literature have been focused on porosity of insect-proof screens as a 2D approach. For instance, Alvarez et al. [21] used a software to estimate the porosity from pictures of screen threads. The porosity is calculated as shown in Equation (13):

$$\phi_{2D} = \frac{A_p}{A_t} = \frac{L_{px} L_{py}}{(L_{px} + D_{hy})(L_{py} + D_{hx})}, \tag{13}$$

where ϕ_{2D} stands for the two-dimensional porosity (in $[m^2/m^2]$ units), A_p is the total pore surface, and A_t is the total area. For instance in [41, 33], this porosity is used to study the effect of ageing and dirt on insect-proof screens. Another important application of this superficial porosity is found in Lopez et al. [23], where this porosity is used to develop models for the aerodynamic performance of insect-proof screens. A similar aerodynamic characterisation is developed by Perez et al. [24] or Castellano et al. [42], amongst many others. Wang and coworkers also analysed computationally in [32] the pressure drop in textile fabrics using 3D models, opposite to the traditional 2D simplified computational approach.

The important drawback implicit in a two-dimensional estimation of porosity is that the effect of the thickness is not taken into account. These works consider the insect-proof screen as a geometry of negligible thickness, and do not consider the thickness of the screen nor the overlap of yarns in the z-coordinate. Thus, a superficial estimation of porosity is an useful but inaccurate

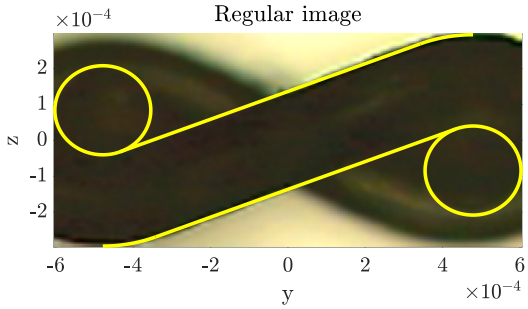

(a) Estimated geometry n.1 in yellow.

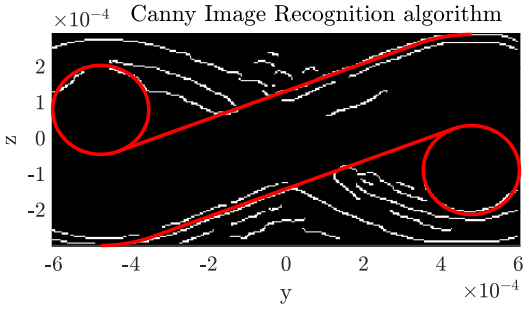

(b) Estimated geometry n.1 in red.

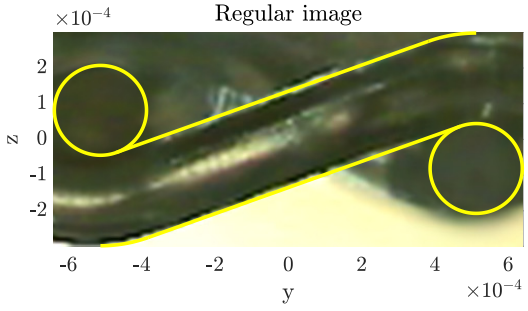

(c) Estimated geometry n.2 in yellow.

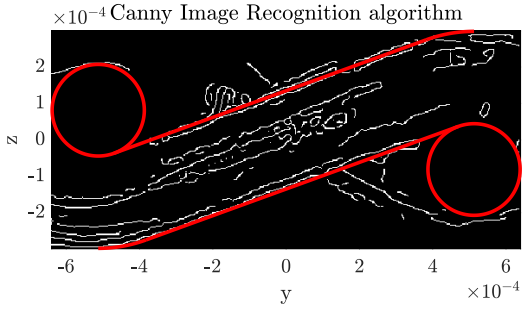

(d) Estimated geometry n.2 in red.

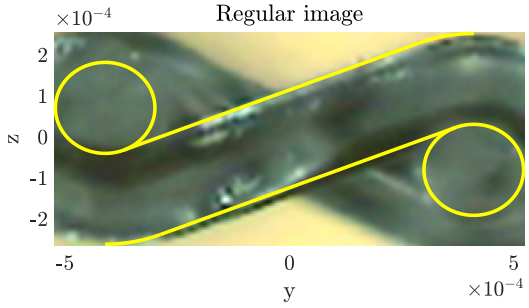

(e) Estimated geometry n.14 in yellow.

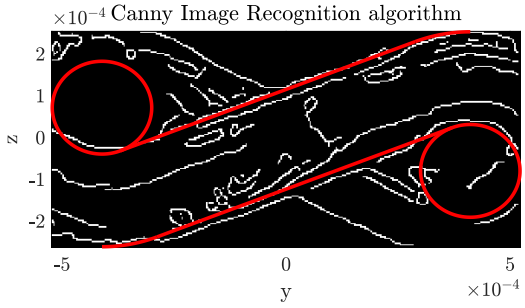

(f) Estimated geometry n.14 in red.

Figure 7: Validation of the estimated geometry of insect-proof screens. The screens are those numbered as n.1 [(a) and (b)], n.2 [(c) and (d)] and n.14 [(c) and (d)] in Lopez et al. [23], as these represent a density of threads of $\rho_t = [11 \times 23]$, $[10 \times 20]$ and $[14 \times 27]$, respectively.

approach to insect-proof screens. The importance of the 3D shape in insect-proof screens has been first considered only in the calculation of the size of the pore in [43]. However, this work only considered the size of the pore as a 2D surface corresponding to the 3D deformation in space of a rectangular pore. They did not provide new estimations of porosity, but suggested that to follow a 3D approach is more accurate.

To estimate a volumetric porosity, the equivalent to superficial porosity can be considered by

calculating the ratio between the volume of the pore and the total volume (see Figure 8):

$$\phi_{3D} = \frac{V_p}{V_t} = 1 - \frac{V_h}{V_t}, \tag{14}$$

where ϕ_{3D} stands for the volumetric porosity (in $[m^3/m^3]$ units), V_p is the total pore volume, V_t is the total volume, and V_h is the total volume filled by the threads. This expression is developed upon the fact that the total volume of the pore can be computed from the difference between the total volume and the volume of the threads. The volumes of the threads are computed straightforward.

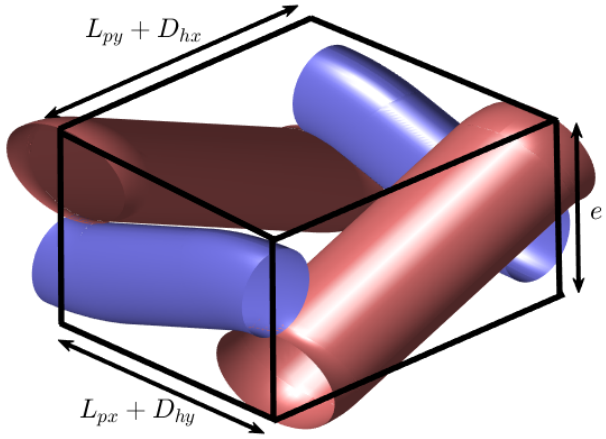

Figure 8: 3D view of the considered volume of the insect-proof screen for the estimation of the volumetric porosity.

The half of the volume of the cylinders are inside the total volume depicted in solid black line in Figure 8. Their volume can be hence computed as $V_{cil} = 1/8\pi D^2 L_i$, with D the diameter of the thread and L_i the length. On the other hand, the volume of the portion of toroid must be computed from integration. Let us consider a generic toroid from Equation (12) but centered in $O(0, 0, 0)$, with $v \in [0, \pi]$ and $u \in [0,\ \theta]$. The volume of the portion of the halved toroid that is developed according to θ can be computed as

$$V_{tor} = \int_0^{\pi} \int_0^{\theta} \int_0^{R} r(a + r\cos v)\, dr\, du\, dv = \frac{1}{2}\pi R^2 a\theta, \tag{15}$$

where the Jacobian has been calculated from

$$J(u, v, R) = \left| \frac{\partial(x',\ y',\ z')}{\partial(u, v, R)} \right| = R(a + R\cos v). \tag{16}$$

Thus, the calculation of the volumetric porosity can be estimated by the code (upon the geometric parameters shown in Figure 2) by including all the volumes in Equation (14) as:

$$\phi_{3D} = 1 - \pi \frac{D_{hx}L_x + D_{hx}^2(D_{hx} + D_{hy})\theta_x + D_{hy}L_y + D_{hy}^2(D_{hx} + D_{hy})\theta_y}{4e(L_{px} + D_{hy})(L_{py} + D_{hx})}, \tag{17}$$

where $e, L_{px}, L_{py}, D_{hx}$ and D_{hy} are inputs given from measurements, and θ_x, θ_y, L_x and L_y are calculated from the inputs by the code. This resulting equation in (17) is interesting not only to provide a three-dimensional porosity upon the said measurements and calculation, but it also enables to estimate the volumetric porosity if θ_x and θ_y are measured at the laboratory from microscope images.

4. Results and Discussion

In this section the models are tested in the estimation of porosity of real insect-proof screens, in order to analyse the differences between a two-dimensional and three-dimensional approach. This includes the application to a large number of screens, as well as a quantification of the impact of ageing in the estimation of both porosities.

4.1. Volumetric Porosity of Insect-Proof Screens

The proposed method to quantify the volumetric porosity in insect-proof screens has been applied to several screens previously measured in the laboratory. Concretely, volumetric porosity has been calculated for 20 insect-proof screens (IPS) from Lopez et al. [23], whose results are provided in Table 1. The 20 IPS selected consist of a set of screens that cover an interesting amount of assorted representative densities of threads (ρ_t) used in Mediterranean greenhouses. A visual comparison between the two-dimensional (ϕ_{2D}) and three-dimensional (ϕ_{3D}) porosities is given in Figure 9. In the figure, data is clustered according to thread density and ordered in ascending order of ϕ_{2D}, which is useful to detect differences in the trend between ϕ_{2D} and ϕ_{3D}. In this figure is observed that there is a notable resemblance in the plot between both porosities (which provides additional confidence in our results), but at the same time volumetric porosity seems to correct certain deficiencies in the superficial porosity approach.

To better understand the goodness of the 3D approach, in Figure 10 is shown the effect of an univariate variation of a $\pm 7\%$ in the thickness of three characteristic IPS of each thread density group ρ_t, the $N_{IPS} = 4$, 16 and 20. In spite of the variation of the thickness does not vary ϕ_{2D}, it is obvious that ϕ_{3D} varies. This increase in thickness can actually generate feasible geometries, as Figures 11 and 12 show for $N_{IPS} = 4$ and 20. It can be observed that, as the thickness is increased, θ_x decreases and θ_y increases (in a screen with *Configuration 1* would happen the opposite), in order to adapt the threads to the new geometry.

N_{IPS}	N (as in [23])	ρ_t	L_{px}	L_{py}	D_{hx}	D_{hy}	e	ϕ_{2D}	ϕ_{3D}
1	15	14×27	131.84	570.46	209.6	225.74	489.82	0.2700	0.6548
2	14	14×27	141.8	615.93	214.81	221.73	514.28	0.2880	0.6876
3	9	14×27	187.33	543.47	186.45	183.97	417.75	0.3790	0.7233
4	26	14×27	188.4	591.6	184.1	184.7	401.7	0.3850	0.7207
5	25	10×20	233.7	734	276.4	273.4	563.8	0.3350	0.6642
6	4	10×20	226.87	681.08	256.83	243.52	566.62	0.3490	0.7092
7	30	10×20	238.57	745.95	272	261.24	564.4	0.3497	0.6877
8	35	10×20	239.99	761.46	263.95	261.81	534.67	0.3541	0.6774
9	3	10×20	232.48	760.74	233.06	253.08	544.35	0.3660	0.7153
10	13	10×20	252.74	746.43	258.95	255.66	639.22	0.3680	0.7453
11	2	10×20	243.71	773.99	251.59	253.5	595.82	0.3690	0.7337
12	12	10×20	250.31	865.1	264.6	260.28	610.55	0.3750	0.7360
13	27	10×20	234.9	838.7	245.8	248	525.91	0.3750	0.7107
14	10	10×20	253.89	784.27	250.54	253.49	586.68	0.3790	0.7351
15	28	10×20	256.6	736.4	256.8	243.7	480.19	0.3790	0.6741
16	8	10×20	246.76	877.27	233.8	236.45	545.95	0.4020	0.7519
17	31	15×30	107.52	456.34	195.99	211.07	507.52	0.2365	0.6626
18	29	13×30	110.02	611.88	187.7	209.4	458.13	0.2634	0.6673
19	22	13×30	170.9	876.8	163.3	160	406.07	0.4370	0.7951
20	17	15×30	221.6	548.8	110.5	109.9	260.57	0.5560	0.8302

Table 1: Estimation of volumetric porosity of 20 representative insect-proof screens in Lopez et al. [23]. All units are given in micrometers (10^{-6} meters). All screens are interlaced according to Configuration 2. N is the number of IPS in [23] and N_{IPS} is the numeration in the present paper.

It is important to note that the increase in thickness has a different impact on each IPS. Whilst a variation of a $\pm 7\%$ in e leads to a relative variation ($\frac{\phi_{3D,max}-\phi_{3D,min}}{\phi_{3D}}$) of a 5.8% for $N_{IPS} = 4$, the impact is halved for $N_{IPS} = 20$, being a 2.9%. For $N_{IPS} = 16$, the impact is a 4.7% of variation. Thus, this illustrates that there are important non-linear interactions between the 3D geometric design parameters and ϕ_{3D} (as expected due to the nature of Equation (14)), opposite to the simplified equation for ϕ_{2D}. This explains the differences in trend of ϕ_{2D} and ϕ_{3D} in Figure 9 and

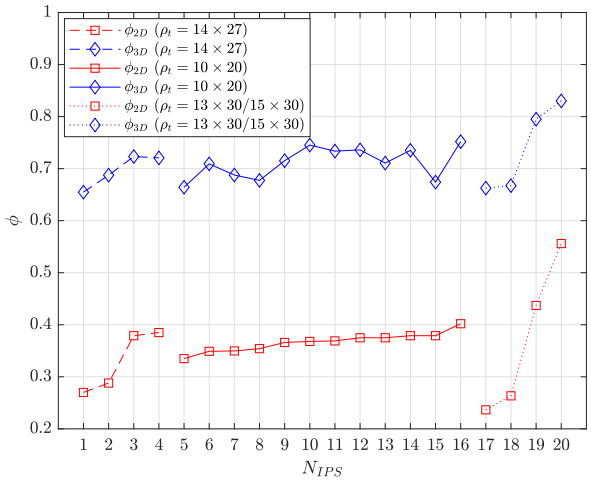

Figure 9: Comparison plot between ϕ_{2D} and ϕ_{3D}.

highlights the importance of a 3D approach for porosity characterisation of insect-proof screens. The sensitivity of ϕ_{3D} to e could be easily obtained analytically from partial derivative of Equation (14) if an analytical solution of θ_x and θ_y is available, which is not the case to our knowledge.

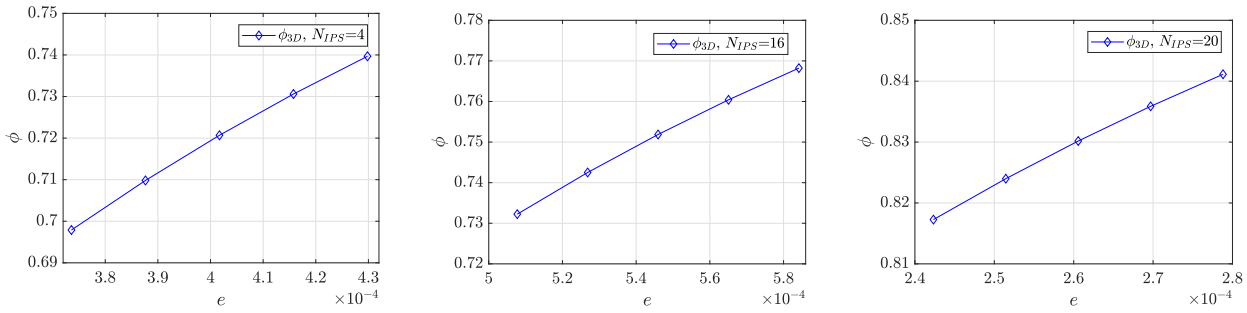

(a) $N_{IPS} = 4$, $\rho_t = 14 \times 27$ (b) $N_{IPS} = 16$, $\rho_t = 10 \times 20$ (c) $N_{IPS} = 20$, $\rho_t = 15 \times 30$

Figure 10: Impact of increasing/decreasing thickness in insect-proof screens.

4.2. Effect of Ageing in the Estimation of Volumetric Porosity

An important issue in insect-proof screens is their deterioration as a consequence of ageing, as pointed out in [33]. The mesh of the screen becomes less tense, thus the diameter of the threads and thickness is slightly increased and the original geometry design suffers some variation. This affects to their aerodynamic behaviour, spotting differences between their new and aged performance [41, 33]. The changes in the structure of the insect-proof screen will thus have an impact on the estimation of the two-dimensional and three-dimensional porosity. Uncertainty in the measurements is also subject to such variability, which is expected to be increased in older

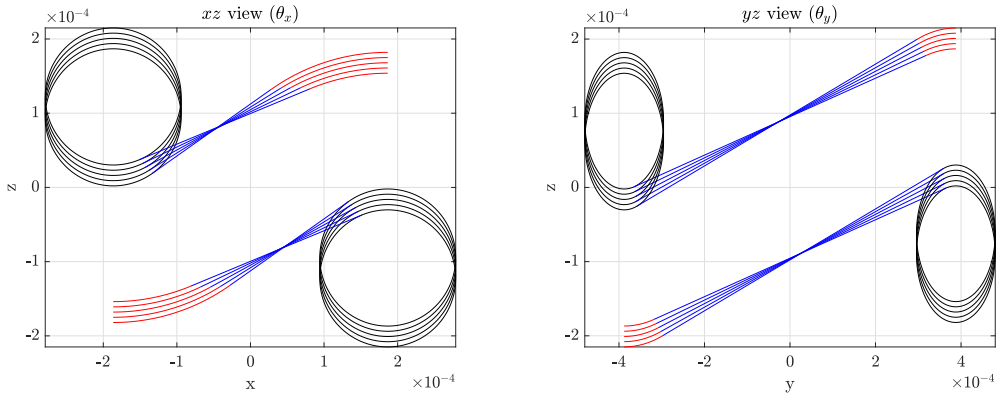

(a) xz view (b) yz view

Figure 11: Impact on geometry of increasing/decreasing thickness in insect-proof screen $N_{IPS} = 4$.

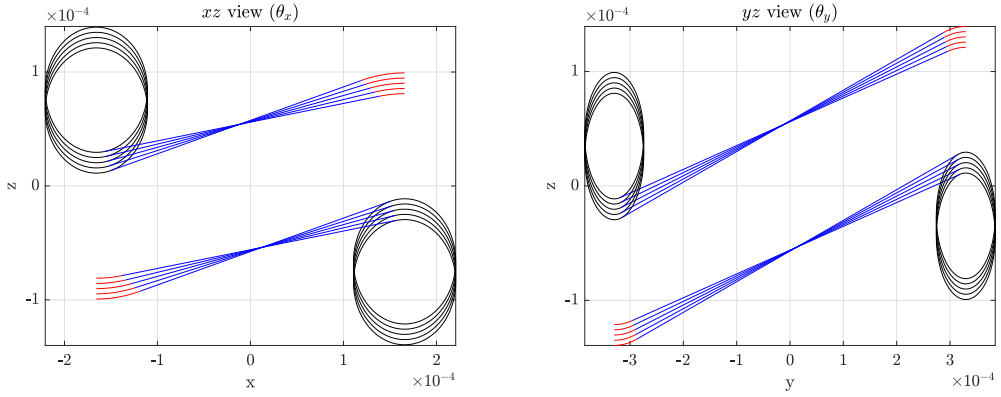

(a) xz view (b) yz view

Figure 12: Impact on geometry of increasing/decreasing thickness in insect-proof screen $N_{IPS} = 20$.

screens. For these reasons, uncertainty quantification can be used to estimate accurately the impact of ageing in the porosity of the insect-proof screen, by including measurement and ageing uncertainty. Although dirt insect-proof screens may be considered for this analysis, the uneven contribution to uncertainty may be misleading, thus this is not considered. Such contribution is uneven in the sense that, for instance, dirt may increase the thickness of the screen, but the diameter of the threads would not be evenly increased (for instance, there is no dirt in the contact surface between threads, etc.). Thence, to study numerically the contribution to uncertainty by dirtiness would not be realistic with our numerical model.

In the present work, the calculation of the insect-proof screen porosity starts with inputs from measurements, and later these are used to calculate the full set of geometric parameters that characterise the screens. However, the impact of uncertainty due to fabrication tolerances, aging

or measurement tolerances may be important in order to quantify the sensitivity of the porosity to the input uncertainty and make a fair comparison. The objective of uncertainty quantification is "to provide confidence measures on how the output of a model is varied due to the variability of its inputs" [44, 45]. This field has gained increasing interest in recent years in applications such as complex fluid dynamics [46], ventilation [47], heat transfer [48], or weather forecasting [49], amongst many others.

The first step in the study of the propagation of uncertainty is to model input uncertainty. For this purpose, realistic random variables have been modelled for e, L_{px}, L_{py}, D_{hx}, and D_{hy}. The measurement data for this modelling corresponds to three insect-proof screens (six studies in total), whose *New* and *Old&Washed* geometric data is provided in [33] (and also in Table 2). According to the central limit theorem, these sources of uncertainty follow a normal distribution, which is written as follows in compact notation for each random variable ξ_i:

$$\xi_i \sim N(\overline{\xi_i},\, \sigma_{\xi i}), \tag{18}$$

where $\overline{\xi_i}$ stands for the mean value of the parameter ξ_i, and $\sigma_{\xi i}$ for the standard deviation of each distribution. This uncertainty quantification has been applied to the six aforementioned insect-proof screens. Upon the modelling of input uncertainty, the five probabilistic distributions of e, L_{px}, L_{py}, D_{hx} and D_{hy} are pseudorandomly sampled with a large number of samples ($N = 20000$) to ensure convergence of the method. It has been tested that this number of samples is enough in our numerical tests. We refer to the sampling as pseudorandom due to the geometric constrains of the problem that lead us to apply constrains to the randomness. Since the sampling is done supposing each parameter as independent, some samples may lead to unfeasible geometries (combinations of the input parameters that do not lead to a realistic geometry) or changes in the configuration (a baseline *configuration 1* may change to *configuration 2* if the size of the threads in the new sample obliges so). These inconveniences can be solved by performing sampling based on relations between the input random variables, but the only relations available are the Equations (1)-(4), which are to be solved in the process. However, it is possible to detect and discard incorrect samples (mathematically possible but physically unfeasible) by taking into account some basic geometric relations. Thus, the sampling has been constrained by the following conditions:

- The maximum thickness that can be achieved in the insect-proof screen is either $2D_{hx} + D_{hy}$ for *configuration 1* (condition 1) or $2D_{hy} + D_{hx}$ for *configuration 2* (condition 2). Thus, in

each sample, either condition 1 or condition 2 must be greater or equal to the actual e in the sample. If this criteria is not matched, the geometry is not realistic.

- The threads are interlaced. Thus, the separation between threads must be at least equal to the diameter of the interlaced thread, otherwise the geometry is not realistic. This is constrained by the relations (see Figure 13): $\frac{h_x}{\sin\gamma_x} - D_{hx} \leq D_{hy}$ and $\frac{h_y}{\sin\gamma_y} - D_{hy} \leq D_{hx}$, where $\gamma_i = atan(\frac{h_i}{L_{pj}+D_{hi}})$ with $i = x, y$.

N (type)	$L_{px} \pm \sigma_{L_{px}}$	$L_{py} \pm \sigma_{L_{py}}$	$D_{hx} \pm \sigma_{D_{hy}}$	$D_{hy} \pm \sigma_{D_{hx}}$	$e \pm \sigma_e$
1 (n)	164.6± 9.3	593.3 ± 19	168.6 ± 6.6	163.1 ± 6.3	391.7 ± 5.3
1 (ow)	156.5 ± 10.7	574.6 ± 19.3	170.5 ± 6	169.3 ± 6	415.6 ± 41.7
2 (n)	234.9 ± 16.1	838.7 ± 27	245.8 ± 7.1	248 ± 8.3	525.9 ± 27.6
2 (ow)	225.8 ± 16.2	828.4 ± 22.5	257 ± 5.3	256.9 ± 8.7	627.9 ± 38.2
3 (n)	256.6 ± 14.3	736.4 ± 17.1	256.8 ± 8.3	243.7 ± 8.2	480.2 ± 11.2
3 (ow)	244.1 ± 15.6	716 ± 23.0	256.7 ± 11.2	252.3 ± 9.4	559.1 ± 50.8

Table 2: Measured geometric parameters (mean value ± standard deviation) of three *New* (n) and *Old&Washed* (ow) insect-proof screens from [33]. All units are given in micrometers (10^{-6} meters).

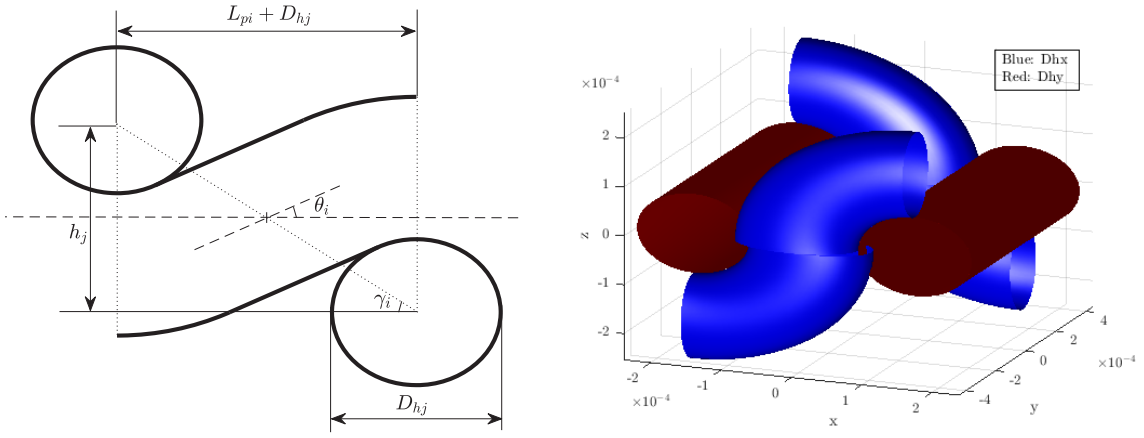

(a) Sketch to quantify the separation between threads.

(b) Example of unfeasible sampled geometry. .

Figure 13: Necessary separation conditions of a sample for a physically permissible geometry.

Due to the uncertainty ranges considered in this work are related to real experimental measurements of clean insect-proof screens, these are not very large. Therefore, it is not frequent to

obtain samples that violate the above mentioned geometric constrains. This usually happened in very few samples in the tail of the probabilistic distributions of the *Old&Washed* screens. Results from the sampling for the insect-proof screen number 1 are shown in Figure 14. The *Old&Washed* screen number 1 was the one with more unfeasible geometries (but only circa 500 out of 20000). In Figure 14 this is noted by observing some cuts in the tail of the distributions of e. As observed, the number of unfeasible geometries is not relevant, but these are discarded from the analysis as their output uncertainty is unreal.

In Figure 15 are depicted the output uncertainty results from the analysis of the same insect-proof screen. It is interesting to note that despite the non-linear relations between input parameters, the output results also follow normal distributions, especially in the *New* insect-proof screens, possibly because the geometry is more robust (lower input uncertainty range, thus less geometries transitioned between *configuration 1* and *2*, no unfeasible geometries discarded, etc.). In Figure 15.(b) can be observed that the *Old&Washed* geometry still preserved the normal distribution shape, but the ϕ_{3D} distribution has certain level of skewness. Must be noted that the distribution of the angle θ_x has its tail cut for $\theta_x < 0$, because unfeasible geometries yield negative values of the angle to satisfy the equations mathematically, but this is not physically correct. It is also observed an important impact on the stochastic standard deviation of relevant parameters such as the angles θ_x and θ_y (in degrees). These parameters exhibit an important range of variation (which is acceptable, as the inclination of the threads is subject to strong variability as the separation and diameters change), which impacts on the calculation of the volumetric porosity.

Finally, the results from this uncertainty analysis for the six screens are shown in Figure 16. In the figure are compared the results of the calculation of superficial and volumetric porosities. In this comparison one can observe an important fact: in the calculation of 2D porosity, the porosity of new screens is greater than the porosity of old and washed screens, as already shown in [33]. However, in the calculation of the volumetric porosity, the scenario is the opposite: the old insect-proof screen porosity is greater than the porosity of new screens. In the works from the literature where new and old screens have been compared, such as [33, 41, 50], they observed that with ageing, the pressure drop of air passing through the screens is decreased in comparison to new insect-proof screens. More concretely, in [33] *New* and *Old&Washed* screens were studied, and it was noticed that the pressure drop was greater for new screens than for the old and washed ones, despite the fact that the (two-dimensional) porosity was greater for new insect-proof screens. The

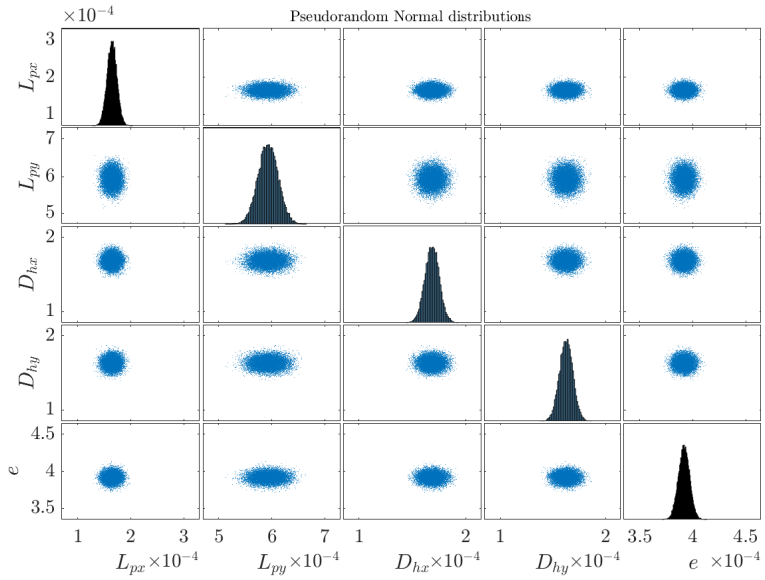

(a) New.

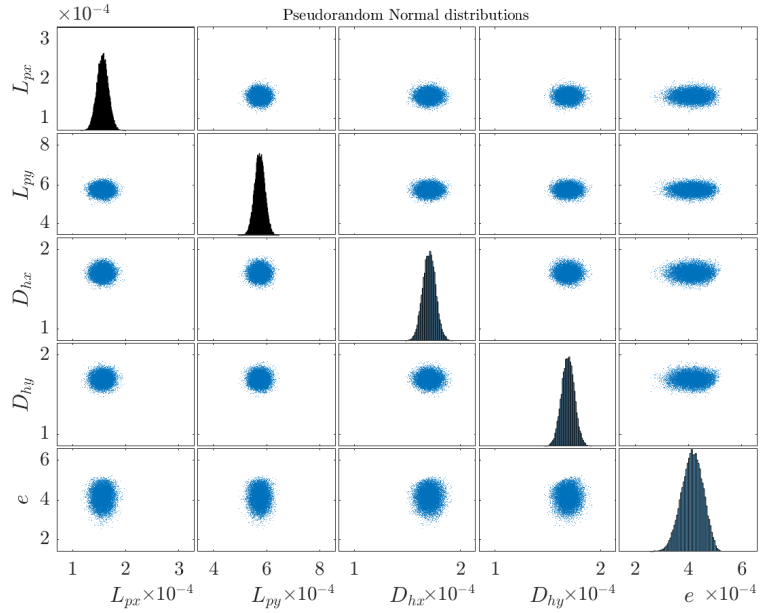

(b) Old&Washed.

Figure 14: Pseudorandom sampling with $N = 20000$ samples for insect-proof screen n.1 from Table 2.

results shown in our analysis thus evidence that ϕ_{3D} is a more realistic representation of porosity of an insect-proof screen, as evidenced in Figure 16. This is evident in the sense that the loss of tension in the threads with time and ageing is assumed to lead to a light increase in the diameter of threads and thickness. The two-dimensional approach does not include any effect of thickness in the porosity, thus the results are doubtful. The calculation shown in this manuscript certifies

the expeced fact that, as the volumetric porosity increases, the pressure drop decreases. Another relevant observation is that the range of variation (uncertainty bars) is more remarkable for the *Old&Washed* screens compared to the *New* screens in the 3D porosity, which may be a result of the greater magnitude of volumetric variations. That is to say, if the radius of a thread is increased, for instance, a 10% in the *Old&Washed* screen due to the lower tension forces, in terms of superficial calculation its increase would be $(1.1R)^2$; whereas the volumetric growth is of order $(1.1R)^3$. Therefore, a volumetric estimation of porosity is also a more complete picture of the impact of ageing in the insect-proof screen in this sense.

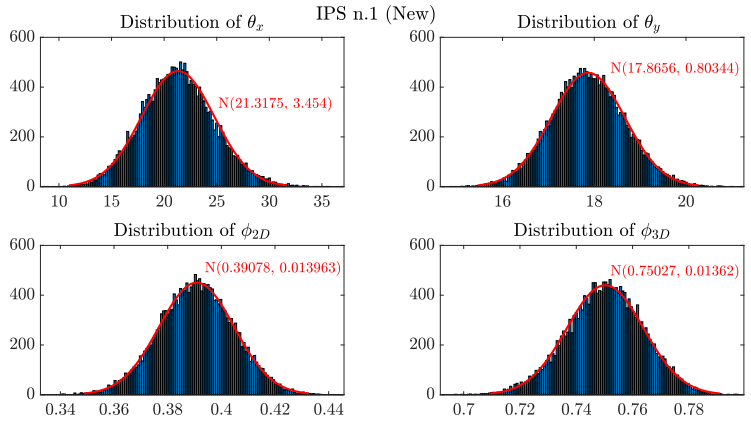

(a) New.

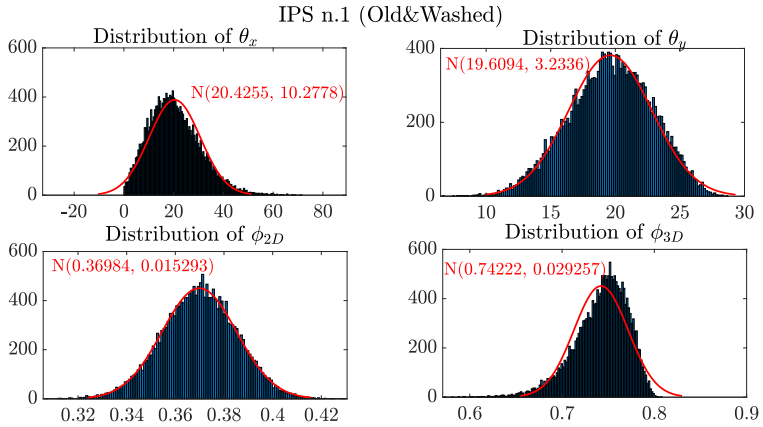

(b) Old&Washed.

Figure 15: Uncertainty quantification results with $N = 20000$ pseudorandom samples and probabilistic distribution fits for insect-proof screen number 1 from Table 2

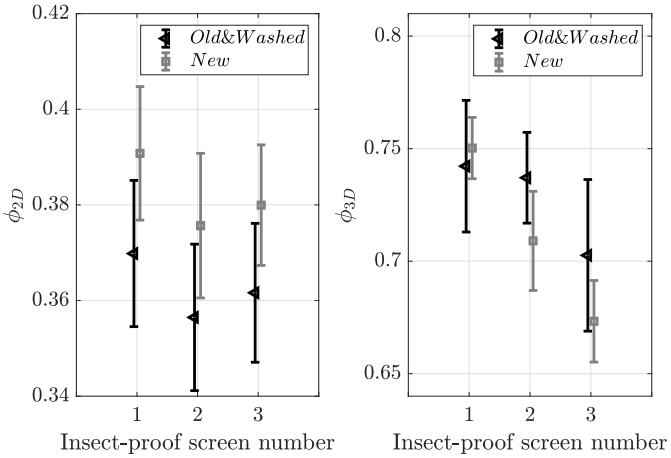

Figure 16: Comparison between *New* and *Old&Washed* insect-proof screens to analyse the effect of ageing in the estimation of porosity. The errorbars are the mean values ± standard deviation. Insect-proof screens from [33] reported in Table 2.

5. Conclusions

A three-dimensional approach is introduced in this work to estimate more accurately the porosity of insect-proof screens from geometric parameters easy to measure. As detected by previous authors, the standard two-dimensional approach in the literature was not able to explain why screens with higher porosity did experience also a greater pressure drop. The introduced approach, which consists of solving a non-linear system of equations and calculate the volume of the threads per total volume, includes the effect of thickness in the estimation of porosity, providing more exact results. The approach allows to reconstruct the three-dimensional geometry computationally, which can be of strong interest to test the aerodynamics of different insect-proof screen designs *à la carte* with Computational Fluid Dynamics codes.

The method has been applied to a total of 20 insect-proof screens, in order to spot the differences between the two and three-dimensional approach. The analysis has shown that non-linear interaction between the geometric variables leads to some differences in the trend of results. In addition, the method has been applied to 6 insect-proof screens to contrast the effect of ageing. In this investigation (which also included a dedicated uncertainty analysis) it has been evidenced that volumetric porosity yields more reasonable results than superficial porosity. This sheds light on the question raised by previous authors on why the expected porosity did not match with the measured pressure drop in brand new and old&washed insect-proof screens. A limitation of the approach is that the non-linear models do not include the effect of tension forces in the variation of the diame-

ter of the threads (which may not be fully circular cross section yarns due to this) nor a potential gentle increase/decrease in thickness, which is future work. Also, it is very important to provide accurate measurements for the computational estimation of the shape of the interlaced threads and porosity. As discussed in the manuscript, if measurements are not correct, the full geometry may not match for obvious reasons (e.g. an incorrectly measured diameter may be larger than the spacing between threads, being an impossible geometry). Additional experimental work dedicated to the observation through microscope and characterisation of an extensive number of manufactured screens (+100) would be very valuable for further validation. Future/current research is also being oriented to the development of aerodynamic models of insect-proof screens, where experimental data of pressure drop in wind tunnels is being used to validate such models. It is expected that models including three-dimensional porosity outperforms those with two-dimensional porosity. Thus, future experimental and modelling work is advisable to further demonstrate the potential of the introduced estimation of three-dimensional porosity.

The methodology and codes resulting from this work have been implemented in the Poro3D v1.0 software, which is provided as supplementary material. The software allows to obtain straightforward both 3D and 2D porosities, as well as the full representation of the 3D geometry.

Supplementary Material

The methodology here developed has been implemented in a software (Poro3D v1.0) to obtain instantly the superficial and volumetric porosity from either manual inputs or Euclides software [21] outputs. The Poro3D v1.0 software is provided as supplementary material to this manuscript, which can be downloaded from the website https://rsoftuma.uma.es/en/software/poro3d/.

Acknowledgments

The authors acknowledge The Andalusian Research, Development and Innovation Plan (PAIDI - Junta de Andalucia) and the research project UAL2020-AGR-A1916 within the FEDER-Andalucia 2014-2020 operational programme.

References

[1] D.L. Valera, L.J. Belmonte, F.D. Molina-Aiz, and A. López. Greenhouse agriculture in almería. a comprehensive techno-economic analysis, Mar 2016.

[2] A.F. Miguel and A.M. Silva. Porous materials to control climate behaviour of enclosures: an application to the study of screened greenhouses. Energy and Buildings, 31(3):195–209, 2000.

[3] Meir Teitel. The effect of insect-proof screens in roof openings on greenhouse microclimate. Agricultural and Forest Meteorology, 110(1):13–25, 2001.

[4] R.A.J Taylor, Sarit Shalhevet, Ishai Spharim, Menachem J Berlinger, and Sarah Lebiush-Mordechi. Economic evaluation of insect-proof screens for preventing tomato yellow leaf curl virus of tomatoes in israel. Crop Protection, 20(7):561–569, 2001.

[5] Meir Teitel. The effect of screened openings on greenhouse microclimate. Agricultural and Forest Meteorology, 143(3):159–175, 2007.

[6] M.J. Berlinger, R.A.J. Taylor, S. Lebiush-Mordechi, S. Shalhevet, and I. Spharim. Efficiency of insect exclusion screens for preventing whitefly transmission of tomato yellow leaf curl virus of tomatoes in israel. Bulletin of Entomological Research, 92(5):367–373, 2002.

[7] Robin V. Gunning and Graham D. Moores. Insensitive Acetylcholinesterase as Sites for Resistance to Organophosphates and Carbamates in Insects: Insensitive Acetylcholinesterase Confers Resistance in Lepidoptera, pages 221–238. Springer Berlin Heidelberg, Berlin, Heidelberg, 2001.

[8] P Muñoz, JI Montero, A Antón, and F Giuffrida. Effect of insect-proof screens and roof openings on greenhouse ventilation. Journal of Agricultural Engineering Research, 73(2):171–178, 1999.

[9] H. Fatnassi, T. Boulard, C. Poncet, and M. Chave. Optimisation of greenhouse insect screening with computational fluid dynamics. Biosystems Engineering, 93(3):301–312, 2006.

[10] Meir Teitel. Using computational fluid dynamics simulations to determine pressure drops on woven screens. Biosystems Engineering, 105(2):172–179, 2010.

[11] Alejandro Lopez-Martinez, Diego L. Valera Martínez, Francisco Molina-Aiz, Araceli Peña-Fernandez, and Patricia Marín-Membrive. Microclimate evaluation of a new design of insect-proof screens in a mediterranean greenhouse. Spanish Journal of Agricultural Research, 12(2):338, 2014.

[12] Peeyush Soni, V.M. Salokhe, and H.J. Tantau. Effect of screen mesh size on vertical temperature distribution in naturally ventilated tropical greenhouses. Biosystems Engineering, 92(4):469–482, 2005.

[13] Harmanto, H.J. Tantau, and V.M. Salokhe. Microclimate and air exchange rates in greenhouses covered with different nets in the humid tropics. Biosystems Engineering, 94(2):239–253, 2006.

[14] C. Kittas, T. Boulard, T. Bartzanas, N. Katsoulas, and M. Mermier. Influence of an insect screen on greenhouse ventilation. Transactions of the ASAE, 45(4), 2002.

[15] F.D. Molina-Aiz, D.L. Valera, A.A. Peña, J.A. Gil, and A. López. A study of natural ventilation in an almería-type greenhouse with insect screens by means of tri-sonic anemometry. Biosystems Engineering, 104(2):224–242, 2009.

[16] Alejandro López, Diego Luis Valera, and Francisco Molina-Aiz. Sonic anemometry to measure natural ventilation in greenhouses. Sensors, 11(10):9820–9838, 2011.

[17] A López, Diego Luis Valera Martínez, Francisco Domingo Molina Aiz, and A Peña. Sonic anemometry measurements to determine airflow patterns in multi-tunnel greenhouses. Spanish Journal of Agricultural Research, (3):631–642, 2012.

[18] Alejandro López-Martínez, Francisco D Molina-Aiz, Diego L Valera-Martínez, Javier López-Martínez, Araceli Peña-Fernández, and Karlos E Espinoza-Ramos. Application of semi-empirical ventilation models in a mediterranean greenhouse with opposing thermal and wind effects. use of non-constant cd (pressure drop coefficient through the vents) and cw (wind effect coefficient). Agronomy, 9(11):736, 2019.

[19] B.J Bailey, J.I Montero, J.Pérez Parra, A.P Robertson, E Baeza, and R Kamaruddin. Airflow resistance of greenhouse ventilators with and without insect screens. Biosystems Engineering, 86(2):217–229, 2003.

[20] Chris Solomon and Toby Breckon. Fundamentals of digital image processing a practical approach with examples in Matlab. Wiley-Blackwell, 2011.

[21] AJ Álvarez, RM Oliva, and DL Valera. Software for the geometric characterisation of insect-proof screens. Computers and electronics in agriculture, 82:134–144, 2012.

[22] V. S. Spiridonov and S. V. Belov. Properties of porous materials composed of metal wire screens with square apertures. i. structural characteristics of materials. Soviet Powder Metallurgy and Metal Ceramics, 24(11):841–845, Nov 1985.

[23] A López-Martínez, FD Molina-Aiz, DL Valera, and KE Espinoza-Ramos. Models for characterising the aerodynamics of insect-proof screens from their geometric parameters. Biosystems Engineering, 192:42–55, 2020.

[24] C Pérez Vega, JA Ramírez Arias, IL López Cruz, et al. Aerodynamic characteristics of anti-insect mesh windows used in greenhouses in mexico. Revista Mexicana de Ciencias Agrícolas, 7(3):493–506, 2016.

[25] R. A. Pinker and M. V. Herbert. Pressure loss associated with compressible flow through square-mesh wire gauzes. Journal of Mechanical Engineering Science, 9(1):11–23, 1967.

[26] A. J. Álvarez, R. M. Oliva, A. Jiménez-Vargas, and M. Villegas-Vallecillos. A three-dimensional approach to the porous surface of screens. The Journal of The Textile Institute, 110(5):639–646, 2019.

[27] Frederick Thomas Peirce. 5—the geometry of cloth structure. Journal of the Textile Institute Transactions, 28(3):T45–T96, 1937.

[28] Bertil Olofsson. 49—a general model of a fabric as a geometric-mechanical structure. Journal of the Textile Institute Transactions, 55(11):T541–T557, 1964.

[29] Zuhaib Ahmad and Brigita Kolčavová Sirková. Analysis of mutual interlacing of threads in multifilament single layer and two layer woven fabric structure using Fourier series. The Journal of The Textile Institute, 2019.

[30] Savvas Vassiliadis, Argyro Kallivretaki, Paraskevas Frantzeskakis, and Christopher Provatidis. Macromechanical modelling of woven fabrics. International Journal of Clothing Science and Technology, 2012.

[31] Savvas Vassiliadis, Argyro Kallivretaki, Dimitra Domvoglou, and Christofer Provatidis. Mechanical analysis of woven fabrics: The state of the art. 2011.

[32] Q Wang, B Maze, H Vahedi Tafreshi, and B Pourdeyhimi. On the pressure drop modeling of monofilament-woven fabrics. Chemical engineering science, 62(17):4817–4821, 2007.

[33] Alejandro López Martínez, Francisco Domingo Molina Aiz, Diego Luis Valera Martínez, Ana Araceli Peña Fernández, and Karlos Espinoza. Effect of material ageing and dirt on the behaviour of greenhouse insect-proof screens. Spanish journal of agricultural research, 16(4):4, 2018.

[34] Luigi Formisano, Antonio Pannico, Christophe El-Nakhel, Giuseppe Starace, Milena Poledica, Stefania De Pascale, and Youssef Rouphael. Improved porosity of insect proof screens enhances quality aspects of zucchini squash without compromising the yield. Plants, 9(10):1264, 2020.

[35] Meir Teitel. Using Computational Fluid Dynamics simulations to determine pressure drops on woven screens. Biosystems engineering, 105(2):172–179, 2010.

[36] M Teitel and E Wenger. Improving airflow through insect-proof screens. In International CIPA Conference 2012 on Plasticulture for a Green Planet 1015, pages 201–207, 2012.

[37] Lei Yang, Xiaoyu Wu, Dewei Zhao, Hui Li, and Jun Zhai. An improved prewitt algorithm for edge detection based on noised image. In 2011 4th International congress on image and signal processing, volume 3, pages 1197–1200. IEEE, 2011.

[38] Wenshuo Gao, Xiaoguang Zhang, Lei Yang, and Huizhong Liu. An improved Sobel edge detection. In 2010 3rd International conference on computer science and information technology, volume 5, pages 67–71. IEEE, 2010.

[39] Shigeru Ando. Consistent gradient operators. IEEE Transactions on Pattern Analysis and Machine Intelligence, 22(3):252–265, 2000.

[40] Rajdeep Dhar, Radheshyam Gupta, and KL Baishnab. An analysis of Canny and Laplacian of Gaussian image filters in regard to evaluating retinal image. In 2014 International Conference on Green Computing Communication and Electrical Engineering (ICGCCEE), pages 1–6. IEEE, 2014.

[41] A López Martínez, Diego Luis Valera Martínez, Francisco Domingo Molina Aiz, Ana Araceli Peña Fernández, and Patricia Marín Membrive. Field analysis of the deterioration

after some years of use of four insect-proof screens utilized in mediterranean greenhouses. Spanish journal of agricultural research, (4):958–967, 2013.

[42] Sergio Castellano, Giuseppe Starace, Lorenzo De Pascalis, Marco Lippolis, and Giacomo Scarascia-Mugnozza. Experimental results on air permeability of agricultural nets. Journal of Agricultural Engineering, 47(3):134–141, 2016.

[43] AJ Álvarez, RM Oliva, A Jiménez-Vargas, and M Villegas-Vallecillos. A three-dimensional approach to the porous surface of screens. The Journal of The Textile Institute, 110(5):639–646, 2019.

[44] Andrea Saltelli, Stefano Tarantola, Francesca Campolongo, and Marco Ratto. Sensitivity analysis in practice: a guide to assessing scientific models, volume 1. Wiley Online Library, 2004.

[45] F-J Granados-Ortiz and J Ortega-Casanova. Quantifying & analysing mixed aleatoric and structural uncertainty in complex turbulent flow simulations. International Journal of Mechanical Sciences, 188:105953, 2020.

[46] Francisco-Javier Granados-Ortiz, Carlos Perez Arroyo, Guillaume Puigt, Choi-Hong Lai, and Christophe Airiau. On the influence of uncertainty in computational simulations of a high-speed jet flow from an aircraft exhaust. Computers & Fluids, 180:139–158, 2019.

[47] Hilde Breesch and Arnold Janssens. Building simulation to predict the performances of natural night ventilation: uncertainty and sensitivity analysis. In Pro. 9th Int. IBPSA Conf, 2005.

[48] F-J Granados-Ortiz, J Ortega-Casanova, and C-H Lai. Propagation of uncertainty in a rotating pipe mechanism to generate an impinging swirling jet flow for heat transfer from a flat plate. Engineering with Computers, pages 1–30, 2020.

[49] Jing Zhao, Yaoqi Duan, and Xiaojuan Liu. Uncertainty analysis of weather forecast data for cooling load forecasting based on the monte carlo method. Energies, 11(7):1900, 2018.

[50] Raphael Linker, Moshe Tarnopolsky, and Ido Seginer. Increased resistance to flow and temperature-rise resulting from dust accumulation on greenhouse insect-proof screens. In 2002 ASAE Annual Meeting, page 1. American Society of Agricultural and Biological Engineers, 2002.